Performance assessment for the linear control of adaptive optics systems: noise propagation and temporal errors

Rémy Juvénal, Caroline Kulcsár, Henri-François Raynaud, Jean-Marc Conan, Gaetano Sivo

HAL Id: hal-01722367

https://hal-iogs.archives-ouvertes.fr/hal-01722367

Submitted on 29 Jun 2023

Performance assessment for the linear control of adaptive optics systems: noise propagation and temporal errors

Rémy Juvénal[a,b], Caroline Kulcsár[a], Henri-François Raynaud[a], Jean-Marc Conan[b], and Gaetano Sivo[c]

[a]Laboratoire Charles Fabry, Institut d'Optique Graduate School, CNRS, Palaiseau, France
[b]ONERA, The French Aerospace Laboratory, F-92322 Châtillon, France
[c]Gemini South Observatory, La Serena, Chile

ABSTRACT

We propose a detailed study of the temporal and noise propagation errors entering the error budget of Single Conjugate Adaptive Optics (SCAO) systems. A transfer-function oriented method is developed for the computation of these errors, in a general linear control context. We apply this formalism to performance comparison between Linear Quadratic Gaussian (LQG) and Integral action controllers. Simulation results are presented, corresponding to a typical SCAO system, in order to validate some approximations on the perturbation power spectral density. We then apply the formalism to evaluate the tip-tilt error budget on GeMS.

Keywords: Adaptive Optics, Error budget, Linear Control, Performance analyses

Introduction

Adaptive optics (AO) systems have taken a key role in diffraction limited astronomical instrumentation for ground based telescopes. However, performance of adaptive optics systems will have to be improved significantly in order to reach the scientific goals of future instruments under development for the VLTs and ELTs. In this context, error budgets are critical tools. Several papers have dealt with the problem of establishing error budgets in the design phase of new AO systems such as the TMT AO system,[3] or the SAXO module of SPHERE.[2] Quirós-Pacheco *et al.*[12] studied the effect of spatial aliasing for integral control with optimized gain, but their method was limited to this particular type of controller. Moreover, error budgets are rarely computed from on-sky data to analyse the performance, but some examples can be found such as CANARY.[15] We propose here, in the special case of a single-conjugate AO (SCAO) configuration, a method which enables to compute the control-dependent terms in the error budget. In the present article, we assume that all the phases can be represented by Zernike modes, which is not restrictive. This method is applicable to any linear controller, and thus can be used to compare the performance of different control laws.

The error budget for SCAO systems is classically expressed as a decomposition of the residual phase variance in a sum of independent terms:

$$\sigma_{\phi^{\text{res}}}^2 = \underbrace{\sigma_{\text{temp}}^2 + \sigma_{\text{alias}}^2 + \sigma_{\text{noise,filt}}^2}_{\text{Control dependent errors}} + \underbrace{\sigma_{\text{fitting}}^2 + \sigma_{\text{NCPA}}^2}_{\text{Control free errors}} \tag{1}$$

We choose to separate these errors into two groups:

(i) The control-dependent errors, which include the temporal error σ_{temp}^2, resulting from the delays in the control loop, the noise propagation error $\sigma_{\text{noise,filt}}^2$, which corresponds to the impact of the wavefront sensor (WFS) measurement noise, and the aliasing error σ_{alias}^2 resulting from WFS (spatial) aliasing.

(ii) The control-free errors, which include the fitting error $\sigma_{\text{fitting}}^2$, related to the finite number of actuators of the deformable mirror (DM), the non common path aberration (NCPA) error σ_{NCPA}^2, due to the differential optical aberrations between the scientific and WFS paths.

In Section 1, we introduce a general transfer function based formalism to describe the control dependent errors, with a focus on the temporal and noise propagation errors. A key ingredient in this calculation is the disturbance (turbulence + vibrations) power spectral density (PSD), which needs to be estimated. In Section 2, we show, with a simplified SCAO simulation, that classical approximations on the structure of the disturbance PSD give acceptable results for SCAO systems. We then illustrate the consistency of this formalism with a performance analysis of tip-tilt on-sky data recorded on the Gemini Multi-Conjugate AO instrument GeMS, evaluating the restrained error budget with the tool defined in previous sections. Finally, we discuss the results presented in this paper, and perspectives for future works.

1. THEORETICAL PERFORMANCE ASSESSMENT

A precise control oriented description of adaptive optics systems has been given by Kulcsár et al.[6] For our purpose, we just need to consider the classical adaptive optics block diagram represented in Fig. 1.
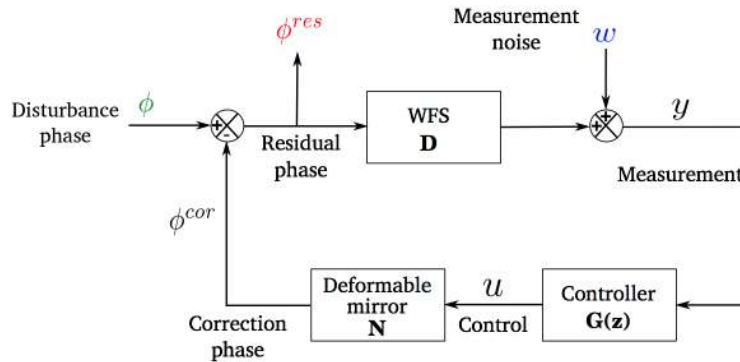

Figure 1: Generic block diagram of an adaptive optics system

Without any limitation to what follows, we can assume a two-frame delay in the system: one frame for WFS integration and another for read-out, centroiding, control computation and data transfer. The system in Fig. 1 has two independent inputs: the disturbance phase ϕ and the measurement noise w ; and one output: the residual phase ϕ^{res}.

1.1 Adaptive optics transfer functions

From an input-output point of view, the diagram in Fig. 1 is completely equivalent to the concise diagram presented in Fig. 2. The two inputs and the output remain the same, but the AO system is completely described by two transfer functions:

- the rejection transfer function T^{rej}, from ϕ to ϕ^{res},

- the noise propagation transfer function T^{noise}, from w to ϕ^{res}.

If we consider a linear controller with transfer function G, we can derive from Fig. 1 the expressions of the AO loop transfer functions:

$$\begin{cases} T^{\text{rej}}(z) = \left[I - z^{-2} N G(z) D \right]^{-1} \\ T^{\text{noise}}(z) = -z^{-1} T^{\text{rej}}(z) N G(z) \end{cases} \tag{2}$$

where N is the deformable mirror influence matrix, D is the WFS matrix and z is the z-transform variable. Using a transfer function, G, is a convenient way to characterize any linear controller, as shown in section 2.1 for LQG and integral controllers.
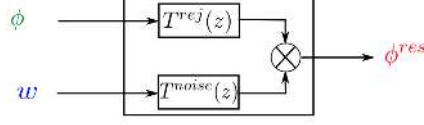

Figure 2: Equivalent SCAO system block diagram

1.2 Theoretical residual phase variance evaluation

Using Parseval's theorem and Fig. 2, we can express the residual phase variance in function of the AO transfer functions:

$$\sigma^2_{\phi^{\text{res}}} = \lim_{T \to \infty} \frac{1}{T} \int_0^T \|\phi^{\text{res}}(t)\|_2^2 \, dt \tag{3}$$

$$= \text{trace} \left(\underbrace{\frac{1}{\pi} \int_0^\pi T^{\text{rej}}(e^{i\omega}) \, S_\phi(e^{i\omega}) \, T^{\text{rej}*}(e^{i\omega}) d\omega}_{\sigma^2_{\text{temp}} + \sigma^2_{\text{alias}} + \sigma^2_{\text{fitting}}} + \underbrace{\frac{1}{\pi} \int_0^\pi T^{\text{noise}}(e^{i\omega}) \, \Sigma_w \, T^{\text{noise}*}(e^{i\omega}) d\omega}_{\sigma^2_{\text{noise,filt}}} \right) \tag{4}$$

where S_ϕ is the PSD of ϕ, and Σ_w is the measurement noise covariance matrix. The second term in the right hand side of equation (4) is an exact expression of the noise propagation error variance. As the measurement noise is generally assumed to be uncorrelated between the WFS subapertures, Σ_w is a diagonal matrix, which is estimated on all operational systems. The first integral in (4) corresponds to the temporal, aliasing and fitting errors.

1.3 Perturbation power spectral density approximation

The first step to evaluate $\sigma^2_{\phi^{\text{res}}}$ using equation (4) is the determination of the disturbance PSD S_ϕ. We use Zernike modes in the following, but any other basis could be used as well. As we do not have access to the perturbation phase on a real system but to WFS measurements, we have to estimate each diagonal component of S_ϕ by reconstructing the associated Zernike modes from the WFS measurements. The least-square reconstructor used for this operation is denoted by R_ϕ and defined as:

$$\begin{aligned} \widehat{\phi} &= R_\phi y, \\ R_\phi &= \left(D^T D\right)^{-1} D^T, \end{aligned} \tag{5}$$

$\widehat{\phi}$ being the reconstructed phase vector, and y the WFS measurement vector.

However, replacing directly the empirical S_ϕ by the PSD $S_{\widehat{\phi}}$ of $\widehat{\phi}$ leads to the propagation of the measurement noise in the rejection transfer function. Thus, in order to compute the true value of the residual phase variance, we have to remove this effect from the residual phase computation and to replace it by the true noise propagation in the AO loop:

$$\sigma^2_{\phi^{\text{res}}} = \text{trace} \left(\frac{1}{\pi} \int_0^\pi T^{\text{rej}}(e^{i\omega}) \, S_{R_\phi y}(e^{i\omega}) \, T^{\text{rej}*}(e^{i\omega}) d\omega \right) - \text{trace} \left(\frac{1}{\pi} \int_0^\pi T^{\text{rej}}(e^{i\omega}) \, R_\phi \Sigma_w R_\phi^{\text{T}} \, T^{\text{rej}*}(e^{i\omega}) d\omega \right)$$
$$+ \text{trace} \left(\frac{1}{\pi} \int_0^\pi T^{\text{noise}}(e^{i\omega}) \, \Sigma_w \, T^{\text{noise}*}(e^{i\omega}) d\omega \right). \tag{6}$$

As $S_{\widehat{\phi}}$, as well as S_ϕ, is a non diagonal matrix-valued function of the frequency ω, its estimation can be computationally demanding. So we also approximate $S_{\widehat{\phi}}$ by a diagonal matrix, neglecting all the correlations between Zernike modes.

2. INTEGRAL/LQG CONTROLLERS COMPARISON IN SIMULATION

In this section, we particularize the error budget formalism developed in Section 1 by comparing integral and Linear Quadratic Gaussian (LQG) controllers with two simulations. First, we simulate in Section 2.2 a simplified SCAO system (without aliasing) in order to demonstrate the consistency of the approximations proposed in Section 1.3. In Section 2.3, we use this method to analyse the performance of the GeMS tip-tilt loop.

2.1 Controllers transfer functions

2.1.1 Integral controller

The integral controller is defined with its recurrence equation:

$$u_k = u_{k-1} + gM_{\mathrm{com}}y_k, \tag{7}$$

where u is the commands vector, g is the integrator gain and M_{com} is the command matrix. Taking the z-transform of equation (7) gives directly the integral controller transfer function:

$$G^{\mathrm{int}}(z) = \frac{gM_{\mathrm{com}}}{1 - z^{-1}}. \tag{8}$$

2.1.2 LQG controller

The LQG control relies on an underlying state space model:

$$\begin{align}
x_{k+1} &= Ax_k + \Gamma v_k, \tag{9}\\
\phi_k &= C_\phi x_k, \tag{10}\\
y_k &= Cx_k - DNu_{k-2} + w_k. \tag{11}
\end{align}$$

The equations (9) and (10) correspond to the perturbation model as the output of a shaping filter, with a white noise v as input. Equation (11) models the WFS measurement process, where C describes the mapping from the state vector x to the WFS measurement vector y and w is the measurement noise. v and w are assumed to be white, Gaussian, and mutually independent, with respectively Σ_v and Σ_w as covariance matrix. LQG control uses a Kalman filter in order to predict the future value of the perturbation through the estimation of the state vector. The structure of an LQG controller, in AO, is given by:

$$\begin{align}
\widehat{x}_{k+1|k} &= A\widehat{x}_{k|k-1} + L\left(y_x - \widehat{y}_{k|k-1}\right) \tag{12}\\
\widehat{y}_{k|k-1} &= C\widehat{x}_{k|k-1} - DNu_{k-2} \tag{13}\\
u_k &= P_u C_\phi \widehat{x}_{k+1|k} \tag{14}
\end{align}$$

where (12) and (13) define a Kalman filter with gain L, where $\widehat{x}$ is the estimated state vector and $\widehat{y}$ is the estimated WFS measurement vector. Equation (14) is the projection of the predicted perturbation on the deformable mirror, P_u being defined as:

$$P_u = N^+ = \left(N^{\mathrm{T}}N\right)^{-1} N^{\mathrm{T}}. \tag{15}$$

The LQG controller transfer function is then obtained by taking the z-transform from equations (12) to (14):

$$G(z) = P_u C_\phi \left(I - (A - LC)z^{-1} - LDNP_u C_\phi z^{-2}\right) L. \tag{16}$$

4

2.2 Multi-mode SCAO simulation

We perform a simplified SCAO simulation in order to validate the approximations suggested in Section 1.3. The disturbance phase has been generated using Auto-Regressive models of order 2 (AR2)[10],[14] using standard observation conditions: observation seeing = 0.7 arcsec, wind velocity norm $V_{\text{wind}} = 15$ m.s^{-1}, damping coefficient $\xi = 0.9$. We simulate an 8 meter VLT telescope. We choose a 10x10 sub-apertures Shack-Hartmann WFS, with a 0.2 rad^2 measurement noise variance (in phase difference at the edge of the sub-apertures), which is representative of high flux observations. The perturbation phase is generated with the 27 first Zernikes modes without piston, according to a Kolmogorov statistics. We limit the number of Zernike modes on purpose in order to avoid any aliasing effect in the simulation. We focus the analysis on the control-dependent error budget. For this reason, we consider a mirror compensating directly all the 27 Zernike modes in order to avoid any fitting error. This way, the total error budget for the simulation is simply given by:

$$\sigma^2_{\phi^{\text{res}}, \text{ simu}} = \sigma^2_{\text{temp}} + \sigma^2_{\text{noise,filt}}. \tag{17}$$

We compare here an integral controller, with a gain of 0.5, and an LQG controller, based on the same AR2 model used to generate the turbulence. In that case, the LQG controller is the optimal (minimum variance) controller. The theoretical performance can be directly computed from equation (4), because all physical quantities are available, particularly the disturbance PSD (including non diagonal elements). Using the integral controller leads to a 0.50 rad^2 theoretical residual phase variance. Using the diagonal approximation proposed in Section 1.3 and estimating the diagonal PSD with WFS measurements, we obtain a 0.51 rad^2 approximated residual phase variance, which corresponds to an error of 2% on the theoretical performance. The LQG controller leads to a 0.25 rad^2 theoretical performance, and to an approximated residual phase variance of 0.27 rad^2, which corresponds to a 8% error. We can push the analysis further by considering the modal decomposition of the theoretical and approximated residual phase variances, with both the approximation and the estimation, represented for the two controllers in Fig. 3. Approximated (red broken line) and theoretical (cyan line) residual phase variance decompositions over the Zernike modes are practically identical. LQG curves are close to each other, but less than for the integral controller ones. Indeed, in the case of the integral controller, we use a diagonal gain – constant here, but an optimized modal gain would not have changed the conclusion – to compute the correction phase. So the diagonal approximation is reflected by the structure of the integral controller, which does not account for the interactions between the modes of the perturbation phase. In the case of the LQG controller, the computation of the Kalman gain accounts for these interactions, so neglecting them leads to a visible error, which is here anyway low as illustrated in Fig. 3.
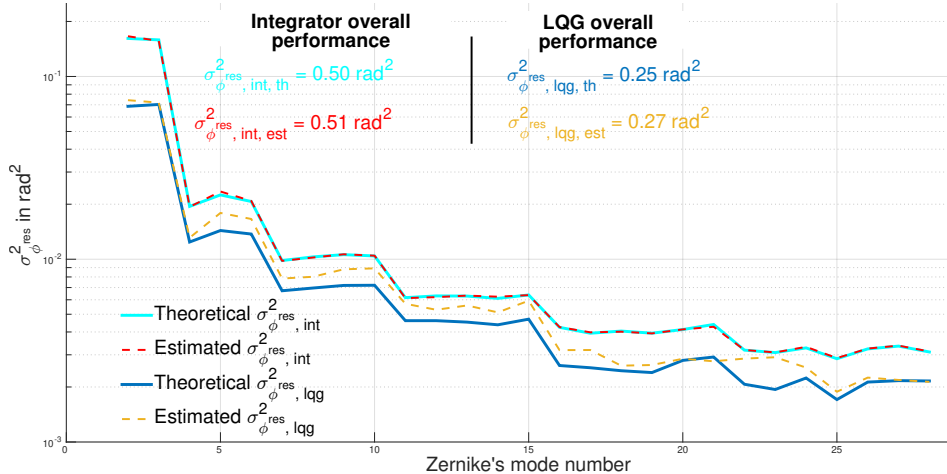

Figure 3: Modal decomposition of the residual phase variances obtained in simulation for LQG and integral controllers. Cyan curve: theoretical integral controller performance; red (dashed) curve: approximated integral controller performance; blue curve: theoretical LQG performance; yellow (dashed) curve: approximated LQG performance.

The LQG controller appears to be twice better in terms of residual variance than the integral controller, which performance would be slightly imroved by increasing the gain g. The pie charts in Fig. 4 represent the error budget decomposition (17) of both controllers for this simulation. We find results close to those presented in Conan *et al.*,[1] using similar simulation conditions. This includes a more balanced compromise between temporal and noise propagation errors for LQG controller. Indeed, the error budget of the integral controller is dominated by the temporal error (90 %). The LQG controller uses a Kalman filter which predicts the perturbation phase one step ahead, with a higher relative impact of the measurement noise than the integral controller.
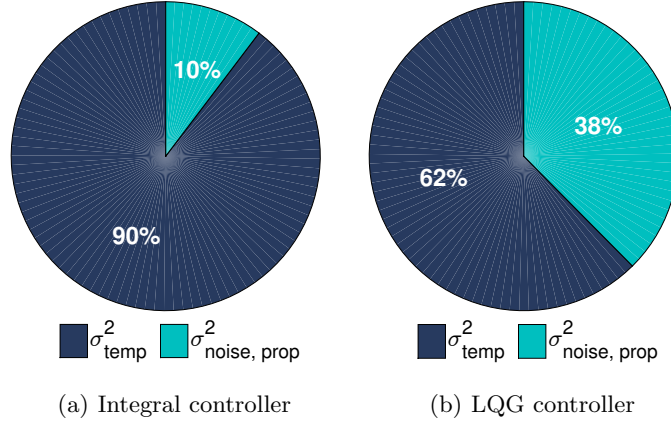

(a) Integral controller   (b) LQG controller

Figure 4: Error budget repartition in simulation restricted to temporal and noise propagation errors comparison.

2.3 Replay simulation with GeMS tip-tilt on-sky data

As the approximations suggested in Section 1.3 have given satisfactory results in simulations, we apply this tool to the performance analysis of on-sky data. We use tip/tilt data from the multi-conjugate AO system GeMS,[9,13] based at Gemini South Observatory, in Chile. The tip/tilt loop of GeMS is actually working exactly like a standard SCAO system. Indeed, the tip/tilt measurements from up to 3 off-axis natural guide stars WFSs are averaged, and the command is computed from this virtual on axis WFS measurements by an integral controller.

GeMS performance, as with most AO systems operating on VLTs, is affected by vibrations. The control law, which is a simple integral controller, cannot efficiently cope with these vibrations. We have collaborated with the GeMS AO team in order to implement an LQG controller with vibration filtering for the tip-tilt loop, the same type of control which was successfully tested on CANARY[14] and which is in operation on SPHERE.[11] As noted in Section 2.1, LQG control relies on an underlying model of the perturbations (turbulence, vibrations, ...). A fine study of these vibrations, and of what would be brought by using an LQG controller using Meimon *et al.*[8] model identification method is presented in Leboulleux *et al.*[7] For example, Fig. 5 represents the PSD of a common buffer from GeMS (black curve), acquired in April 2015. We can see a particularly intense vibration around 37Hz. We have studied several model identification methods[4] in order to find the most suitable technique for the GeMS tip/tilt loop. The identification method used to compute the results presented below is called cPEM[5] (for cascaded Prediction Error Minimization) and has provided the best results during the study. The green curve on Fig. 5 shows the PSD of the model, identified from half of the buffer.
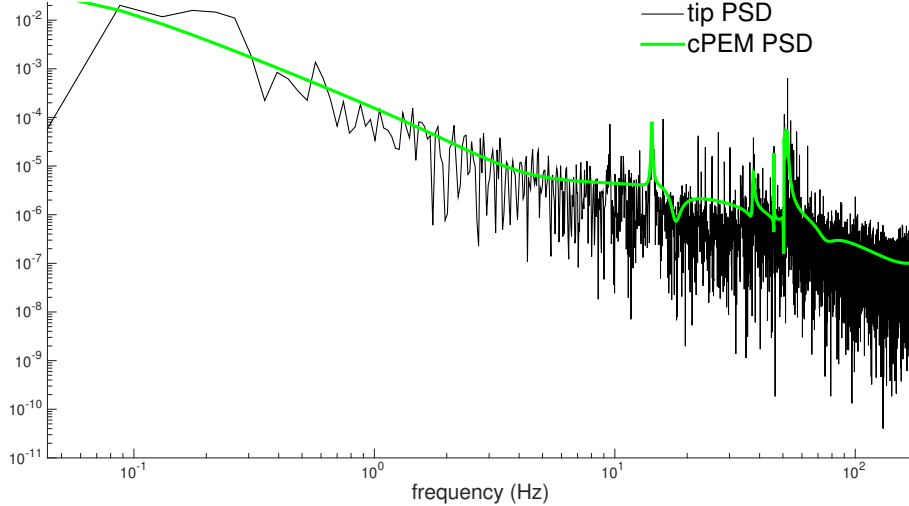
Figure 5: PSD of tip from buffer ngs15108223248, acquired in April 2015 with GeMS. Black curve: sample empirical PSD. Green curve: PSD of the model identified with cPEM.

Before discussing the results, note that when using pseudo open-loop data to simulate an AO loop (replay mode), the residual phase variance evaluation is different from that of section 2.3. Indeed, we have access here neither to the real perturbation phase, nor to the measurement noise values to run the simulation, but only to the WFS measurements. The residual phase obtained is therefore in this case:

$$\widehat{\Phi}^{\mathrm{res}}(z) = T^{\mathrm{rej}}(z)R_\phi Y(z) = T^{\mathrm{rej}}(z)R_\phi \left(D\Phi(z) + W(z)\right) = T^{\mathrm{rej}}(z)R_\phi D\Phi(z) + T^{\mathrm{rej}}(z)R_\phi W(z), \qquad (18)$$

where Φ^{res}, Y, Φ and W are the z-transforms of respectively the residual phase ϕ^{res}, the WFS measurements y, the perturbation phase ϕ and the measurement noise w. Therefore, in order to compute the correct residual phase variance (see eq. (4)), we have to remove from the residual phase variance evaluated in replay-mode the measurement noise filtered by the rejection transfer function and to add the impact of the noise propagation:

$$\sigma^2_{\phi^{\mathrm{res}}} = \sigma^2_{\widehat{\phi}^{\mathrm{res}}} - \sigma^2_{\mathrm{noise}} \int \left\| T^{\mathrm{rej}} R_\phi \right\|^2 + \sigma^2_{\mathrm{noise, \, filt}}. \qquad (19)$$

From (19), we evaluate the error budget of the integral controller, illustrated in Fig. 6(a), and of the LQG controller obtained from the cPEM identified model, illustrated in Fig. 6(b). The integral controller overall performance (here in on-sky angle, *i.e.* in residual phase standard deviation) is 19.4 mas and 15.4 mas for the LQG controller. The LQG performance is for this buffer around 25 % lower than for the integral controller (see Juvénal *et al.*[4] for more details). Looking at the error budget decomposition, we note first that the integral controller is completely dominated by the temporal error. The LQG controller achieves, again, a better RMS compromise between the two errors, compromise that is essential here in presence of vibrations. We can note that the temporal error is, however, largely dominant in the LQG error budget (95%). This is due to 2 phenomena:

- first, the measurement noise level was very low for this observation, *i.e.* the natural guide stars were bright (the operating point is a classical high-flux observation),

- secondly, the identified model, due to real-time control constraints, is limited to 15 cells of order 2. The perturbation model is consequently limited to the representation of 14 vibration peaks. Therefore, some small unfiltered vibrations can remain uncorrected, and impact the error budget of the LQG controller.

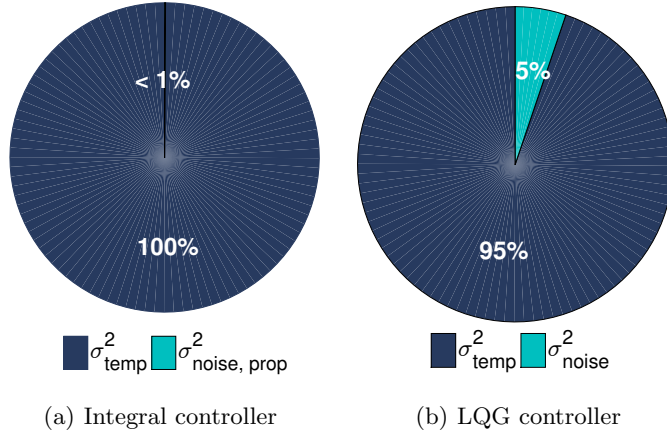(a) Integral controller   (b) LQG controller

Figure 6: Error budget repartition in replay mode with GeMS on-sky tip-tilt data. Buffer ngs15108223248 (tip), April 2015, evaluation made on the last 4000 samples, 350 Hz, 3 natural guide stars.

3. CONCLUSION

We have presented in this paper a general formalism for the control-dependent error budget evaluation, applicable for any SCAO system and any linear controller. We aim at designing a tool that allows accurate comparisons between controllers. The critical element of this error budget evaluation process is the estimation of the disturbance PSD, due to the lack of knowledge about the disturbance in a real system. We show that we can use reasonable approximations to evaluate the performance of a SCAO system. The first simulation verifies the validity of both the approximation and the estimation for the residual phase estimation. We can also use this formalism to study how any linear controller would perform on a specific system, by estimating its overall performance and evaluating all the terms in its error budget. This allows to determine on which aspects a controller should be improved. We still need to model finely the impact of WFS aliasing for SCAO systems, which is an on-going work. A clue to achieve this is to study the modal structure of both the rejection and noise propagation transfer functions. The next step is to evaluate the control-dependent error budget terms for Wide-field Adaptive Optics systems, which will require the description of other errors like the tomographic error, together with special attention to the disturbance PSD estimation.

Acknowledgements

REFERENCES

[1] J.-M. Conan, H.-F. Raynaud, C. Kulcsár, S. Meimon, and G. Sivo. Are integral controllers adapted to the new era of ELT adaptive optics? In *AO4ELT2*, 2011.

[2] T. Fusco, G. Rousset, J.-F. Sauvage, C. Petit, J.-L. Beuzit, K. Dohlen, D. Mouillet, J. Charton, M. Nicolle, M. Kasper, P. Baudoz, and P. Puget. High-order adaptive optics requirements for direct detection of extrasolar planets: Application to the SPHERE instrument. *Optics Express*, 14, June 2006.

[3] L. Gilles, L. Wang, and B. Ellerbroek. Wavefront Error Budget Development for the Thirty Meter Telescope Laser Guide star Adaptive Optics System. *Adaptive Optics Systems, SPIE proceedings*, June 2008.

[4] R. Juvénal, C. Kulcsár, H.-F. Raynaud, J.-M. Conan, C. Petit, L. Leboulleux, G. Sivo, and V. Garrel. Tip-tilt modeling and control for GeMS: a performance comparison of identification techniques. In *AO4ELT4*, 2015.

[5] C. Kulcsár, P. Massioni, G. Sivo, and H.-F. Raynaud. Vibration mitigation in adaptive optics control. *Adaptive Optics Systems III, SPIE Proceedings*, July 2012.

[6] C. Kulcsár, H.-F. Raynaud, C. Petit, and J.-M. Conan. Minimum variance prediction and control for adaptive optics. *Automatica*, pages 1939–1954, Sept. 2012.

[7] L. Leboulleux, G. Sivo, R. Juvénal, C. Kulcsár, V. Garrel, J.-M. Conan, H.-F. Raynaud, C. Petit, W. Rambold, E. Marin, and V. Montes. Vibration analysis on gems tip-tilt data and performance evaluation using an LQG controller. In *AO4ELT4*, 2015.

[8] S. Meimon, C. Petit, T. Fusco, and C. Kulcsár. Tip-tilt disturbance model identification for kalman-based control scheme: application to XAO and ELT systems. *JOSA A*, 27:122–132, Nov. 2010.

[9] B. Neichel, F. Rigaut, F. Vidal, M.-A. van Dam, V. Garrel, E. Rodrigo Carrasco, P. Pessev, C. Winge, M. Boccas, C. d'Orgevilles, G. Arriagada, A. Serio, V. Fesquet, W. Rambold, J. Lührs, C. Moreno, G. Gausachs, R. Galvez, V. Montes, T. Vucina, E. Marin, C. Urrutia, A. Lopes, S. Diggs, C. Marchant, A. Ebbers, C. Trujillo, M. Bec, G. Trancho, P. McGregor, P. Young, F. Colazo, and E. Michelle. Gemini multi-conjugate adaptative optics system review II: Commissioning, operation and overall performance. *Monthly Notices of the Royal Astronomical Society*, pages 1002 – 1019, May 2014.

[10] C. Petit. *Development of a new control law for the adaptive optics facility (AOF)*. ONERA/DOTA/HRA, 2011.

[11] C. Petit, J.-F. Sauvage, T. Fusco, A. Sevin, M. Suarez, A. Costille, A. Vigan, C. Soenke, D. Perret, S. Rochat, et al. Sphere eXtreme AO control scheme: final performance assessment and on sky validation of the first auto-tuned LQG based operational system. In *SPIE Astronomical Telescopes+ Instrumentation*, page 91480O. International Society for Optics and Photonics, 2014.

[12] F. Quiros Pacheco, J.-M. Conan, and C. Petit. General aliasing and its implications in modal gain optimization for multi-conjugated adaptive optics. *JOSA A*, 27:A182–A200, Nov. 2010.

[13] F. Rigaut, B. Neichel, M. Boccas, C. d'Orgeville, F. Vidal, M. A. van Dam, G. Arriagada, V. Fesquet, R. L. Galvez, G. Gausachs, C. Cavedoni, A. W. Ebbers, S. Karewicz, E. James, J. Lührs, V. Montes, G. Perez, W. N. Rambold, R. Rojas, S. Walker, M. Bec, G. Trancho, M. Sheehan, B. Irarrazaval, C. Boyer, B. L. Ellerbroek, R. Flicker, D. Gratadour, A. Garcia-Rissmann, and F. Daruich. Gemini multiconjugate adaptive optics system review - I. design, trade-offs and integration. *Monthly Notices of the Royal Astronomical Society*, 437 (3):2361 – 2375, Jan. 2014.

[14] G. Sivo, C. Kulcsár, J.-M. Conan, H.-F. Raynaud, E. Gendron, A. Basden, F. Vidal, T. Morris, S. Meimon, C. Petit, D. Gratadour, O. Martin, Z. Hubert, A. Sevin, D. Perret, F. Chemla, G. Rousset, N. Dipper, G. Talbot, E. Younger, R. Myers, D. Henry, S. Todd, D. Atkinson, C. Dickson, and A. Longmore. First on-sky SCAO validation of full LQG control with vibration mitigation on the CANARY pathfinder. *Optics Express*, 22:23565–23591, 2014.

[15] F. Vidal, E. Gendron, G. Rousset, T. Morris, A. Basden, R. Myers, M. Brangier, F. Chemla, N. Dipper, D. Gratadour, D. Henry, Z. Hubert, A. Longmore, O. Martin, G. Talbot, and E. Younger. Analysis on on-sky MOAO performance of CANARY using natural guide stars. *Astronomy & Astrophysics*, 569, Sept. 2014.